Nitrifier adaptation to low energy flux controls inventory of reduced nitrogen in the dark ocean

Yao Zhang[a,b,1], Wei Qin[c], Lei Hou[a,b], Emily J. Zakem[d], Xianhui Wan[a], Zihao Zhao[e], Li Liu[a,b], Kristopher A. Hunt[f], Nianzhi Jiao[a,b], Shuh-Ji Kao[a,b], Kai Tang[a,b], Xiabing Xie[a], Jiaming Shen[a,b], Yufang Li[a,b], Mingming Chen[a,b], Xiaofeng Dai[a,b], Chang Liu[a,b], Wenchao Deng[a], Minhan Dai[a,b], Anitra E. Ingalls[c], David A. Stahl[f], and Gerhard J. Herndl[e,g]

[a]State Key Laboratory of Marine Environmental Sciences, Xiamen University, 361101 Xiamen, China; [b]College of Ocean and Earth Sciences, Xiamen University, 361101 Xiamen, China; [c]School of Oceanography, University of Washington, Seattle, WA 98195; [d]Department of Biological Sciences, University of Southern California, Los Angeles, CA 90089; [e]Department of Limnology and Bio-Oceanography, Center of Functional Ecology, University of Vienna, A-1090 Vienna, Austria; [f]Department of Civil and Environmental Engineering, University of Washington, Seattle, WA 98195; and [g]Department of Marine Microbiology and Biogeochemistry, Royal Netherlands Institute for Sea Research, Utrecht University, 1790 AB Den Burg, The Netherlands

Edited by Paul G. Falkowski, Rutgers University, New Brunswick, NJ, and approved January 25, 2020 (received for review July 18, 2019)

Ammonia oxidation to nitrite and its subsequent oxidation to nitrate provides energy to the two populations of nitrifying chemoautotrophs in the energy-starved dark ocean, driving a coupling between reduced inorganic nitrogen (N) pools and production of new organic carbon (C) in the dark ocean. However, the relationship between the flux of new C production and the fluxes of N of the two steps of oxidation remains unclear. Here, we show that, despite orders-of-magnitude difference in cell abundances between ammonia oxidizers and nitrite oxidizers, the two populations sustain similar bulk N-oxidation rates throughout the deep waters with similarly high affinities for ammonia and nitrite under increasing substrate limitation, thus maintaining overall homeostasis in the oceanic nitrification pathway. Our observations confirm the theoretical predictions of a redox-informed ecosystem model. Using balances from this model, we suggest that consistently low ammonia and nitrite concentrations are maintained when the two populations have similarly high substrate affinities and their loss rates are proportional to their maximum growth rates. The stoichiometric relations between the fluxes of C and N indicate a threefold to fourfold higher C-fixation efficiency per mole of N oxidized by ammonia oxidizers compared to nitrite oxidizers due to nearly identical apparent energetic requirements for C fixation of the two populations. We estimate that the rate of chemoautotrophic C fixation amounts to ~1×10^{13} to ~2×10^{13} mol of C per year globally through the flux of ~1×10^{14} to ~2×10^{14} mol of N per year of the two steps of oxidation throughout the dark ocean.

nitrification | dark ocean | nitrogen flux | carbon fixation | homeostasis

The ocean represents the largest reservoir of reactive nitrogen (N) on Earth, containing about five times more bioavailable N than terrestrial systems (1). Populations of chemoautotrophic microorganisms living in the energy-starved dark ocean (below the sunlit layer) exploit reduced inorganic N supplied by sinking organic matter to fuel chemosynthesis, resulting in the accumulation of nitrate, the fully oxidized form of N that fuels new production in the ocean when deep water masses upwell into the energy-rich sunlit zone. While there are reports of complete nitrification activity in a single organism (comammox) in terrestrial systems (2–4), in the oceans, the conversion of ammonia (hereafter defined as combined ammonia and ammonium) to nitrate is thought to be exclusively controlled by a partnership between ammonia- and nitrite-oxidizing microorganisms.

It is assumed that nitrite oxidation is tightly coupled to ammonia oxidation in the ocean, as nitrite is always present at concentrations approximately equal to ammonia and one to three orders of magnitude lower than nitrate, suggesting a rapid consumption of nitrite once it is made available (5–7). Two exceptions are the primary nitrite maximum at the base of the euphotic zone (8) and the secondary nitrite maximum in the oxygen minimum zone (9). Ammonia-oxidizing archaea (AOA), assigned to the phylum *Thaumarchaeota*, are thought to control ammonia oxidation to nitrite in oligotrophic conditions because of their significantly higher affinity for ammonia (e.g., the half-saturation constant K_m of *Nitrosopumilus maritimus* is ~132 nM total ammonia) (10) compared to ammonia-oxidizing bacteria. These observations suggest that marine nitrite-oxidizing bacteria (NOB), among which populations of *Nitrospina* and *Nitrospira* are most ubiquitous (11–14), have similarly high affinities for nitrite. However, cultured representatives of NOB mainly originate from non-oxygenated oceanic environments, and their K_m values are orders of magnitude higher than those of marine AOA (10, 15–22). Only one recent study showed that the half-saturation constant K_s (254 ± 161 nM) for nitrite oxidation is of the same magnitude as that of marine AOA in the low-oxygen seawater of the Eastern

Significance

Carbon fixation in the dark ocean is sustained primarily by nitrifying populations, providing new organic matter to heterotrophic food webs. However, the flux of new carbon through nitrification, controlled by the coupling of the highly divergent ammonia- and nitrite-oxidizing microbial assemblages at depth, remains unclear. We here constrain the flux by combining depth-related population data with kinetic and process-level measurements in a thermodynamic framework and then demonstrate consistency between our observations and theoretical balances from an ecosystem model. We estimate that a balanced flux (homeostasis) of nitrogen passing between the two populations fuels ~1×10^{13} to ~2×10^{13} mol of C per year carbon fixation in the energy-limited dark ocean.

Author contributions: Y.Z., W.Q., D.A.S., and G.J.H. designed research; L.H., E.J.Z., X.W., Z.Z., L.L., K.A.H., X.X., J.S., Y.L., M.C., X.D., and C.L. performed research; Y.Z., W.Q., L.H., E.J.Z., X.W., Z.Z., L.L., K.A.H., N.J., S.-J.K., K.T., X.X., J.S., Y.L., M.C., X.D., C.L., W.D., M.D., and A.E.I. analyzed data; Y.Z., W.Q., E.J.Z., D.A.S., and G.J.H. wrote the paper; and E.J.Z. analyzed the steady state model balances and comparisons with data.

The authors declare no competing interest.

This article is a PNAS Direct Submission.

Data deposition: The metatranscriptomics datasets were deposited in the National Center for Biotechnology Information Short Reads Archive, https://www.ncbi.nlm.nih.gov/sra (accession nos. SRR5518753, SRR5515070, and SRR5518752). The transcriptome shotgun assembly project was deposited at the DNA Data Bank of Japan/European Molecular Biology Laboratory/GenBank databases (accession no. GGEF00000000). The Fortran code for the MATLAB code for the thermodynamic analyses are available at GitHub (https://github.com/emilyzakem/ZhangLabXMU).

[1]To whom correspondence may be addressed. Email: yaozhang@xmu.edu.cn.

This article contains supporting information online at https://www.pnas.org/lookup/suppl/doi:10.1073/pnas.1912367117/-/DCSupplemental.

First published February 18, 2020.

Tropical North Pacific (ETNP) (23), where nitrite concentrations are in the micromolar range, suggesting that the K_s for nitrite might be even lower in oceanic regions with lower nitrite concentration. Nitrite-oxidation kinetics in the ocean are poorly constrained relative to the substrate affinity for ammonia-oxidation processes, hindering understanding and efforts to model the homeostatic N cycle that fuels much of the energy-limited dark ocean.

Although the two steps of nitrification are assumed to be tightly coupled and, thus, at a steady state, oxidation of nitrite yields less energy than the oxidation of ammonia (5), which leads to less bioavailable energy to fuel chemoautotrophic growth by nitrite oxidation in the dark ocean. However, recent studies reported that dark ocean carbon (C) fixation by marine NOB is unexpectedly much higher than that by AOA (11), suggesting that marine NOB assimilate inorganic C via a far more energy-efficient autotrophic pathway than the 3-hydroxypropionate/4-hydroxybutyrate (HP/HB) C-fixation cycle in AOA or utilize additional sources of energy for C fixation.

We sought to resolve these confounding explanations and clarify the flux of C fixed through nitrification by combined environmental and culture-based analyses. We performed a comprehensive analysis of ammonia and nitrite oxidation in the South China Sea (SCS) and the Western Pacific Ocean (WP) (*SI Appendix*, Fig. S1), combining gene- and transcript-level analyses with a kinetic analysis of ammonia- and nitrite-oxidation rates. Those studies were then complemented by a corresponding characterization of pure cultures of marine AOA and NOB to determine cell-specific rates of ammonia and nitrite oxidation and dissolved inorganic C (DIC) fixation. Combining the culture-based measurements with in situ data, we estimated the apparent DIC-fixation efficiency normalized with the oxidized N and consumed energy by AOA and NOB. Finally, to investigate the broader implications of our findings, we synthesized our observations of rates, kinetics, and efficiencies with steady-state balances from a microbial ecosystem model with explicit descriptions of nitrifying populations. This synthesis revealed a mechanistic basis for the matched flux of N through each of the two steps of oxidation and, in addition, that affinity-matched coupling of the two populations acts to maintain nitrite at consistently low concentrations.

Results and Discussion

Disparity in C-Fixation Efficiencies per N Oxidation between Marine AOA and NOB. As has been found in many parts of the oceans (12, 13), AOA were one to two orders of magnitude more abundant than NOB (sum of *Nitrospira* and *Nitrospina*; Wilcoxon, $P < 0.01$) in the SCS and WP (*SI Appendix*, Fig. S2 *A–C* and *SI Texts* S1–S3). Based on the striking differences in abundance between AOA and NOB in the ocean, DIC fixation and, hence, biomass production might be expected to differ substantially between AOA and NOB. We examined the stoichiometric relations between DIC fixation and ammonia versus nitrite oxidation using cultures of *N. maritimus* SCM1, *Nitrospira moscoviensis* NSP M-1, and *Nitrospina gracilis* 3/211 at temperatures similar to vast areas of the ocean's epipelagic waters (*SI Appendix*, Fig. S3 and *SI Text* S4). The cell-specific nitrite-oxidation rates of NSP M-1 and 3/211 were two-fold and 10-fold higher, respectively, than cell-specific ammonia-oxidation rates of SCM1 (*SI Appendix*, Fig. S3 *C*, *G*, and *K*). The cell-specific oxidation rates measured in the cultures closely resembled the average cell-specific oxidation rates of AOA and NOB determined in the oceanic water column (Table 1). The cell-specific DIC-fixation rates of SCM1 were similar to those of NSP M-1 and 3/211 (*SI Appendix*, Fig. S3 *C*, *G*, and *K*). Taken together, the measured activities confirmed the expected higher C yield per N oxidized of SCM1 than in all NOB strains (*SI Appendix*, Fig. S3 *D*, *H*, and *L*). The culture-based DIC-fixation efficiency of marine AOA based on our analysis of strain SCM1 and a previous analysis of three additional marine strains (24) (Fig. 1) was 3.4 times higher than that of the NOB *Nitrospira* and *Nitrospina* (0.0729 versus 0.0216 mol of C fixed per mol of N oxidized) (Fig. 1). This ratio of 3.4 is supported by the ratio of free energy available from ammonia oxidation and nitrite oxidation of ~3.7 under standard conditions (5), as well as the almost identical (1.1 versus 1) apparent energy requirements (unit energy consumption per mol of C fixed) of the thaumarchaeotal HP/HB C fixation and the reductive tricarboxylic acid (rTCA) cycle operational in *Nitrospira*- and *Nitrospina*-like NOB. This ratio is in agreement with the

Table 1. Ammonia and nitrite oxidation and DIC-fixation rates

Zone	Surface	Euphotic zone	Bottom of euphotic zone	Upper mesopelagic zone	Lower mesopelagic zone
Depth (m)	25	50 to 150	200 to 300	350 to 450	500 to 1,000
PAR	99.80	65.40 to 1.13	0.14 to 0	0	0
NH_4^+ (nM)†	88	46.63	30	30.25	25.30
NO_2^- (nM)†	10	91.63	56.25	18.50	19.65
NO_3^- (μM)†	0.07	2.12	2.76	12.33	34.67
NH_4^+ oxidation rate (nM N per d)†	0.11	17.91	8.56	0.42	0.05
NO_2^- oxidation rate (nM N per d)†	0.01	9.27	9.48	3.53	0.12
Archaeal *amoA* gene abundance (10^5 copies per L)*,†	0.02	31.12	24.38	15.04	12.01
NOB 16S rRNA gene abundance (10^5 copies per L)*,†	0.07	2.53	2.47	1.55	1.42
NH_4^+ oxidation rate per cell (fmol of N per cell per d)	55.08	5.76	3.51	0.28	0.04
NO_2^- oxidation rate per cell (fmol of N per cell per d)	1.25	36.64	38.38	22.77	0.85
Estimated AOA DIC-fixation rate (nM C per d)	0.008	1.31	0.62	0.03	0.004
Estimated NOB DIC-fixation rate (nM C per d)	0.0002	0.20	0.20	0.08	0.003

^{15}N-labeled ammonium (NH_4^+) and nitrite (NO_2^-) oxidation rates, archaeal *amoA* gene and NOB (sum of *Nitrospira* and *Nitrospina*) 16S rRNA gene abundances, and estimated AOA and NOB DIC-fixation rates at site W2 in the WP. PAR, photosynthetically active radiation in μmol of photons per $m^2 \cdot s^{-1}$.
*$P < 0.05$, AOA *amoA* gene and NOB 16S rRNA gene abundance were positively correlated to NH_4^+ and NO_2^- oxidation rate, respectively.
†Data were depth-weighted averages of the corresponding zone.

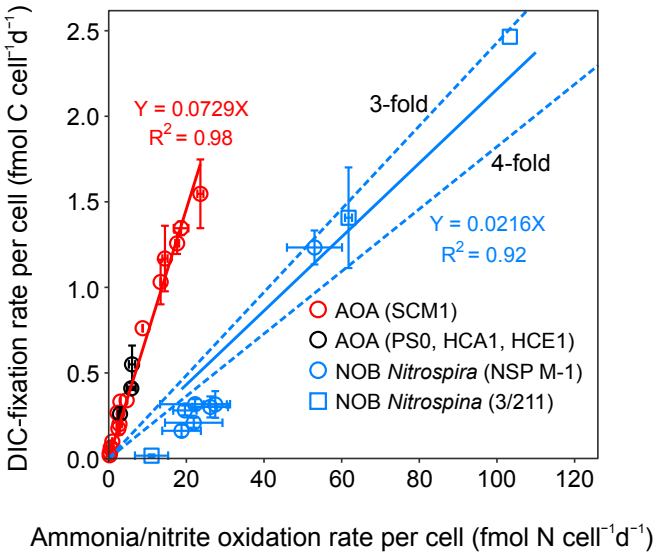

Fig. 1. Activity parameters of selected AOA and NOB strains determined under controlled laboratory conditions. Additionally, three marine AOA strains (*Nitrosopumilus ureaphilus* PS0, *N. cobalaminigenes* HCA1, and *N. oxyclinea* HCE1) determined in a previous study are added (24). Means ± SDs are given. The error bars represent SDs of biological replicates (n = 3). One square representing *Nitrospina* has no SDs, as culture volumes are very small, and biological replicates are not available. Stoichiometric relationships (type I regression) between cell-specific ammonia and nitrite oxidization and DIC-fixation rates are obtained. The two blue dashed lines indicate the theoretical predictions of efficiencies from Zakem et al. (25) (with a slope threefold lower than the red regression line) and the thermodynamic free energy (with a slope fourfold lower).

redox-based prediction of Zakem et al. (25) of a threefold difference in biomass N synthesis yield per mol of dissolved inorganic N (DIN) used between AOA and NOB.

Since the C-fixation rates of AOA and NOB reflect the energy available from the respective nitrification redox reactions, the rates should be sensitive to the ambient concentrations of the DIN species. For example, because of the significant accumulation of nitrate at depth (up to 37 μM), nitrite oxidation is expected to be energetically less favorable in the deep ocean than in the upper ocean, as nitrate concentrations are in the submicromolar to low-micromolar range in surface waters (Table 1). Accordingly, we modeled the change in relative free energy of these two consecutive nitrification reactions in shallow and deep waters with distinct concentrations of DIN (*SI Appendix*, *SI Text S5*). We found that the relative free energy available for the two reactions in the upper oceans is congruent with the theoretical values calculated under the standard condition (~3.7 J/J for ammonia relative to nitrite oxidation). In contrast, as nitrate concentration increases and nitrite concentration decreases in the dark ocean, ammonia oxidation may yield nearly 4.5 times more energy than nitrite oxidation (*SI Appendix*, Fig. S4), a 20% increase in relative yield. Taking the minor difference of the apparent energetic requirements for DIC fixation (1.1 versus 1) of AOA and NOB into account, the DIC-fixation efficiency of AOA per N oxidation is up to ~4.1 times higher than that of the NOB populations in the dark ocean. Taken together, the culture-based experiments, previous theoretical and empirical estimates (25), as well as the thermodynamic calculations reveal an approximately threefold to fourfold higher DIC-fixation efficiency in AOA than for NOB *Nitrospira* and *Nitrospina* in the ocean (Fig. 1).

Homeostasis of Ammonia and Nitrite Oxidation. Ammonia- and nitrite-oxidation rates measured by using ^{15}N-labeled compounds (Table 1 and *SI Appendix*, Fig. S5) indicated that bulk ammonia-oxidation rates were higher than nitrite oxidation in the epipelagic zone (25 to 150 m; Wilcoxon, $P < 0.05$). Below the epipelagic zone, however, the inferred bulk nitrite-oxidation rates were higher than the bulk ammonia-oxidation rates (Wilcoxon, $P < 0.05$; Table 1). Similar observations of higher nitrite-oxidation capacity in the mesopelagic layer have also been made in the North Atlantic Ocean (26, 27) and Southern California Bight (28, 29) by using the ^{15}N tracer method. This suggests that ammonia oxidation is the rate-limiting step in nitrification, and, in the mesopelagic layer, NOB have the potential to immediately oxidize the nitrite produced from ammonia oxidation so that the two nitrification steps become tightly coupled in the ocean's interior. Thus, our observations confirm the assumption that homeostasis is maintained, which we define here as balanced (relatively equal) ammonia- and nitrite-oxidation rates (*Materials and Methods*). Only time-varying pulses of organic matter (30) might result in an ephemeral decoupling of the two steps, resulting in nitrite accumulation, if ammonia-oxidization rates increase more than nitrite oxidization through a rapid response to increased concentrations of ammonia.

Since the production of nitrite at depth is mainly controlled by the rate of ammonia oxidation (25), and the concentration of nitrite decreases with depth and diminishing ammonia concentration, we anticipated that the affinity of NOB for nitrite would increase with depth. The affinity was estimated by using Michaelis–Menten kinetics of ammonia oxidation (*SI Appendix*, Fig. S6) and nitrite oxidation (Fig. 2). Remarkably, the in situ K_s values for nitrite oxidation were orders of magnitude lower than the K_m values of cultured representatives and varied over an order of magnitude between depths of 75 and 200 m in the SCS (Fig. 3). The low K_s values for nitrite oxidation (K_s = 27 to 506 nM) are comparable to those for in situ ammonia oxidation previously reported in the Eastern Tropical South Pacific (ETSP) (27.2 ± 4.4 nM) (15), Puget Sound Hood Canal (98 ± 14 nM) (16), Sargasso Sea (65 ± 41 nM) (17), and the SCS (60.6 to 167.6 nM) (18) as well as in the present study (80.9 ± 66.4 nM) (Fig. 3). Notably, the K_s values of both in situ ammonia and nitrite oxidation decreased with depth overall (Fig. 2 and *SI Appendix*, Fig. S6). The kinetic constants were extended to mesopelagic waters by using simple models of an exponential fit of these measurements, suggesting exceptionally low in situ K_s values at depth that were undetectable by the $^{15}NH_4^+$/$^{15}NO_2^-$ isotope technique (*SI Appendix*, Fig. S7 *A* and *B*). These analyses confirm the inherent capacity for in situ coupling of these two nitrification steps. Coupling was consistent with measured in situ abundance data, showing that archaeal *amoA* and NOB 16S rRNA gene abundances were positively correlated to the ammonia-oxidation (R = 0.88, $P < 0.05$) and nitrite-oxidation (R = 0.94, $P < 0.05$) rates, respectively (Table 1). Thus, nitrifying populations at depth have a potential to draw down both ammonia and nitrite to very low concentrations (*SI Appendix*, Fig. S7).

Consistency of Observed Nitrification Homeostasis with Model Predictions. We compared the observations with theoretical balances from a model of the nitrification ecosystem (ref. 25 and *Materials and Methods*) to gain further insight into the activities and loss rates of the nitrifying populations in the dark ocean. As outlined in Zakem et al. (25), the steady-state concentrations (subsistence resource concentrations R^*) of ammonia and nitrite at depth can be expressed as functions of the uptake affinities, yields (mol of biomass synthesized per mol of N oxidized), and loss rates of the nitrifier populations in accordance with resource-competition theory (*Materials and Methods*). The biomass yields are directly proportional to the DIC-fixation efficiencies (mol of C fixed per mol of N oxidized). Our measurements indicate that, at a given depth in the ocean, both in situ affinities and concentrations of ammonia are of similar magnitude to the in situ

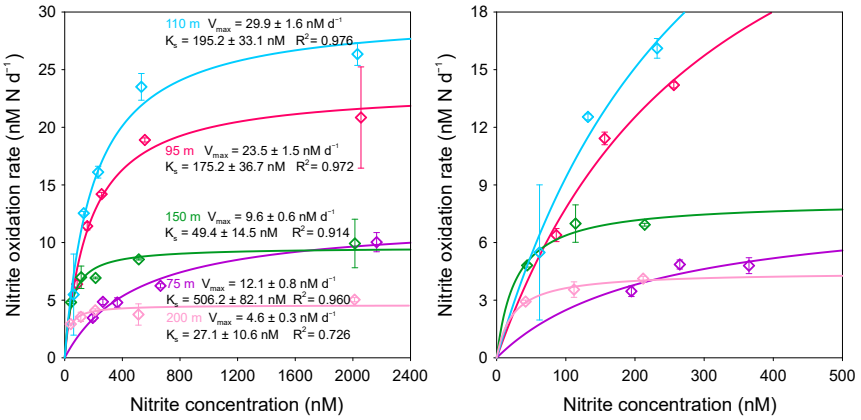

Fig. 2. Michaelis–Menten kinetics of nitrite oxidation. Nitrite-oxidation rates were measured at different substrate concentrations at five depths between 75 and 200 m of site S6 in the SCS. Measured rates were obtained from the slope of the linear regression of six independent time-course bottles (*SI Appendix, Materials and Methods*). Error bars represent the SE of the regression coefficient. The solid lines were fitted by using the Michaelis–Menten equation. R^2, coefficients (V_{max} and K_s) of the best fit, and their SEs are shown. (*Left*) Shows all the data; (*Right*) shows the range 0 to 500 nM NO_2^- concentration.

affinities and concentrations of nitrite (Fig. 3 and Table 1). Additionally, the observed DIC-fixation efficiency is threefold to fourfold higher for ammonia oxidizers than for nitrite oxidizers (Fig. 1), indicating that AOA can yield threefold to fourfold more biomass than NOB for the same amount of N oxidation, which is consistent with the theoretical threefold difference in yield and maximum growth rate from the redox-based model (*Materials and Methods*). We use R^* to further predict that the threefold to fourfold difference in efficiency must be compensated by a three-time-higher loss rate in order to obtain the same ammonia and nitrite concentrations at depth as observed here. We speculate that an approximately

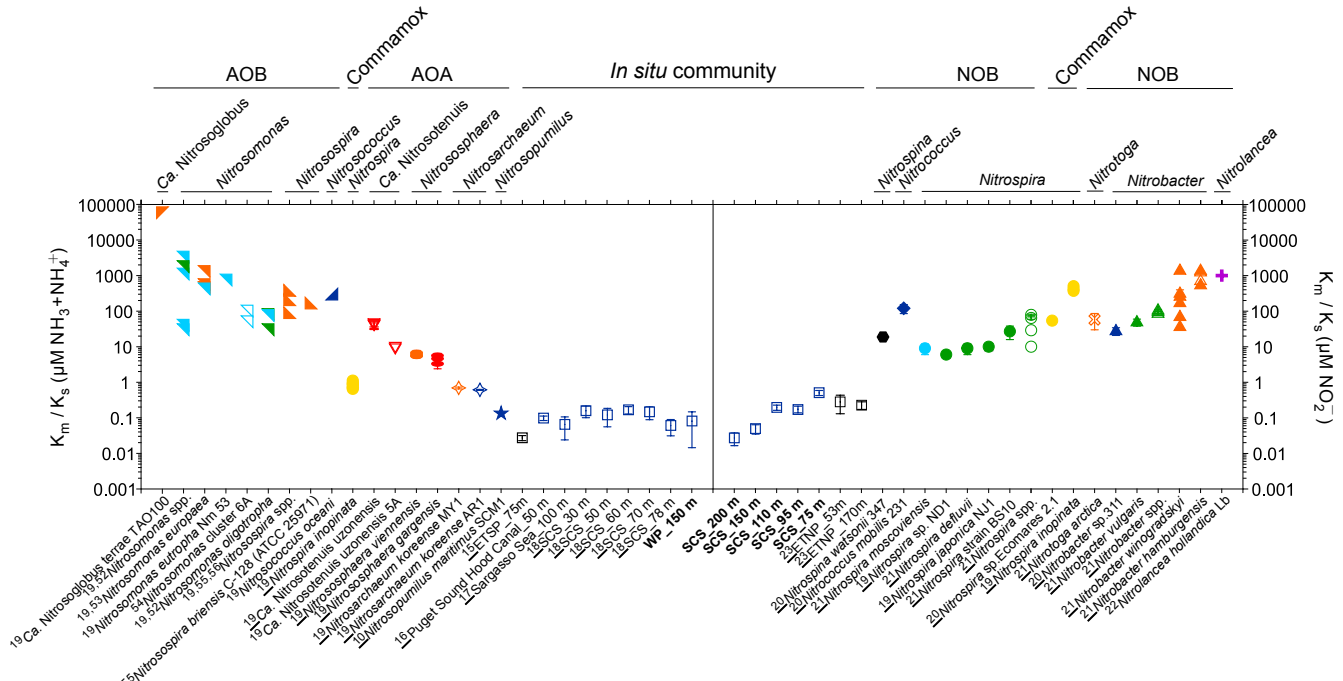

Fig. 3. Ammonia affinities of AOA and ammonia-oxidizing bacteria (AOB) and nitrite affinities of NOB. K_m (K_s) values of members of the genera *Ca.* Nitrosoglobus (upper left triangle) (19), *Nitrosomonas* (upper right triangles) (19, 52–54), *Nitrosospira* (lower left triangles) (19, 55, 56), *Nitrosococcus* (lower right triangle) (19), *Nitrospira* (comammox) (circles) (19), *Ca.* Nitrosotenuis (down-pointing triangles) (19), *Nitrososphaera* (ellipses) (19), *Nitrosarchaeum* (stars) (19), and *Nitrosopumilus* (pentacle) (10), and in situ communities (squares) from the ETSP (15), Puget Sound Hood Canal (16), Sargasso Sea (17), SCS (18), and the WP (this study is marked in bold; the error bar represents the SE of the estimated coefficient) for ammonia oxidation are shown on the left; K_m (K_s) values of members of the genera *Nitrospina* (hexagon) (20), *Nitrococcus* (diamond) (20), *Nitrospira* (circles) (19–21), *Nitrotoga* (fork) (21), *Nitrobacter* (triangles) (20, 21), *Nitrolancea* (cross) (22), and in situ communities (squares) from the ETNP (23) and the SCS (this study is marked in bold; error bars represent the SE of the estimated coefficient) for nitrite oxidation are shown on the right. Cultures were derived from ocean (dark blue), oceanic oxygen-deficient water (black), freshwater (light blue), activated sludge (green), soil (orange), biofilm (yellow), bioreactor (purple), and hot spring/well water (red). Filled symbols indicate pure culture; open symbols indicate mixed culture/enrichment or in situ community. *Ca.*, *Candidatus*. The values obtained from refs. 19 and 21 are also from references in the two articles. –, the error bars are obtained from references.

threefold higher loss rate of the AOA relative to NOB might be caused by higher mortality or maintenance requirements at depth. In support of this speculation, recent marine viral metagenomic studies report that the AOA *amoC* is common in marine viral genomes (31, 32). This suggests that AOA, as one of the most abundant and ubiquitous microbes in the ocean, are frequently infected and lysed by marine viruses. In contrast, the much lower abundance of NOB may result in less grazing pressure and viral lysis than in AOA. This assumption is supported by the experiments performed in both mesocosms and in situ. It has been shown in oceanic surface sediments that the impact of viral infection is higher on *Thaumarchaeota* than on bacteria, accounting for up to one-third of the total microbial biomass lysed (33).

Our observations (Table 1 and *SI Appendix*, Figs. S2 *A–C* and S5) confirm the predictions made by the redox-informed ecosystem model of higher abundances of AOA relative to NOB, as well as of the equal rates of ammonia and nitrite oxidation in the dark ocean. Specifically, estimated differences in yield and in cell size (10-fold higher N cell quota for NOB than AOA) (25) predict at least an order of magnitude higher abundance of AOA relative to NOB (*Materials and Methods*), which is consistent with our observed difference of one to two orders of magnitude. The similar ammonia- and nitrite-oxidation rates, both observed and theoretically predicted, indicate that the rates of the sequential steps of nitrification are largely set by the flux of sinking organic N into the deeper layers of the ocean (refs. 17, 25, 29, 34, and 35 and *Materials and Methods*).

Dark C Fixation Maintained by Ammonia and Nitrite Oxidation. Applying C-fixation efficiency parameters for AOA and NOB to the in situ ammonia- and nitrite-oxidation rates, 0.4 to 3.1 times higher bulk dark DIC-fixation rates of ammonia than nitrite oxidizers were obtained for the mesopelagic waters of the WP (Table 1). Furthermore, the depth profiles of ammonia- and nitrite-oxidation rates below the euphotic zone of the WP and SCS were fitted into the Martin curve by using a power-law equation (36) (*SI Appendix*, Fig. S5). Globally integrated ammonia and nitrite oxidation are $1.61 \pm 0.25 \times 10^{14}$ mol of N per year (mean ± 95% CI) and $2.28 \pm 0.53 \times 10^{14}$ mol of N per year, respectively, by extrapolating the WP values to the entire volume of the ocean below the euphotic zone (*SI Appendix*, *Materials and Methods*), and $1.3 \pm 0.33 \times 10^{14}$ mol of N per year and $1.37 \pm 0.07 \times 10^{14}$ mol of N per year by extrapolating the SCS values. This translates into a global oceanic DIC fixation of 1.2×10^{13} mol of C per year for AOA and 0.5×10^{13} mol of C per year for NOB based on the in situ ammonia- and nitrite-oxidation rates at the WP and 0.9×10^{13} mol of C per year for AOA and 0.3×10^{13} mol of C per year for NOB based on the in situ oxidation rates at the SCS. These global ammonia-oxidation rates below the euphotic zone represent ∼40 to ∼50% of the N released (3.3×10^{14} mol of N per year) (37) by mineralization of global export production (2.2×10^{15} mol of C per year) in the mesopelagic and bathypelagic zones of the ocean (38). Thus, these global rates of dark-ocean DIC fixation by ammonia oxidizers are around half of the estimate, assuming that all ammonia generated from mineralization in the ocean's interior is oxidized by AOA. The other half of the released N is probably assimilated by the heterotrophic food web and/or removed through denitrification or anammox in the oxygen minimum zones. These C-fixation rates are also in close agreement with the global simulation of Zakem et al. (25), which estimates that total DIC fixation associated with ammonia oxidation and nitrite oxidation is 1×10^{13} and 0.26×10^{13} mol of C per year, respectively. In the simulation, the approximately fourfold, rather than approximately threefold, difference is due to the fact that the higher maximum growth rate of ammonia oxidizers allows them to more efficiently compete with phytoplankton for DIN in the lower epipelagic waters.

The relative contributions of marine AOA and NOB to total DIC fixation in the dark ocean have also been inferred from single-cell analyses in the western North Atlantic (11). Pachiadaki et al. (11) estimated that the global dark-ocean DIC fixation by NOB is one order of magnitude higher than that by AOA. However, extremely unbalanced ammonia and nitrite fluxes would be required to establish such relationships of DIC fixation reported by Pachiadaki et al. (11), which would essentially break the homeostatic balance of nitrification in the dark ocean. Our data suggest that the nitrite oxidation-based autotrophy contributes only a minor fraction to the total DIC fixation and thus biomass production of NOB in the dark ocean. However, as catalyzed reporter deposition-fluorescence in situ hybridization combined with microautoradiography analyses provide estimates of C fixation derived from all possible energy sources, it is possible that the higher DIC fixation of NOB is supported by other unidentified energy sources.

Our metatranscriptomic analysis indicated that the dark-ocean NOB might be metabolically flexible. In addition to the highly expressed transcripts involved in nitrite oxidation (*SI Appendix*, *SI Text S6*), notably, transcripts of genes for sulfur oxidation were abundant in the *Nitrospira*-affiliated metatranscriptome at 200-m depth, and transcripts of the genes encoding the carbon monoxide dehydrogenase (CODH) were abundant in the metatranscriptome of *Nitrospina* from 200- and 3,000-m depth (Fig. 4 and *SI Appendix*, Tables S1 and S2). *Nitrospina*-affiliated CODH genes were also actively expressed in metatranscriptomes from the ETSP and ETNP (39, 40). Since aerobic CODHs might oxidize carbon monoxide (CO) (41), CO could serve as an alternative energy source for NOB. However, given the rather low free energy available from CO oxidization (−20 $kJ \cdot mol^{-1}$) (42), it is unlikely that CO could support significant chemoautotrophic growth of NOB. DIC fixation with biogenic sulfur compounds as energy source is estimated to be about 10× lower than DIC fixation from nitrification (table 3 in ref. 43). We therefore consider that NOB production may be up to about 10% higher if NOB carry out all of this sulfur oxidation. This higher yield and a lower yield from thermodynamic effects at depth (*SI Appendix*, Fig. S4) constrained the lower (2.7-fold) and upper (4.1-fold) boundaries of the relative DIC-fixation efficiencies between AOA and NOB under the homeostatic control of the overall nitrification process in the dark ocean. These analyses also point toward unaccounted-for energy sources supporting DIC fixation at depth.

Taken together, our findings indicate a substantial ecophysiological disparity between marine AOA and NOB. AOA are more abundant, with smaller cell sizes and lower cell-specific N-oxidation rates than NOB. The lower cell-specific ammonia-oxidation rates of AOA as compared to the cell-specific nitrite-oxidation rates of NOB are compensated by the higher abundance of AOA, resulting in similar bulk ammonia-and nitrite-oxidation rates in the oceanic water column. However, more free energy available from ammonia oxidation than nitrite oxidation results in three to four times higher DIC-fixation efficiency in AOA than in NOB *Nitrospira* and *Nitrospina* due to the nearly equal apparent energy requirements of their DIC fixation. Our observations confirm the redox-based prediction of an approximately threefold higher maximum growth rate of the AOA than NOB, and we speculate that an approximately threefold higher loss rate of AOA than NOB may also differentiate the populations. In addition, the affinities of both AOA and NOB for ammonia and nitrite, respectively, are similar and increase with depth and substrate limitation. Therefore, the equal affinities, the approximately threefold-higher efficiency, and an approximately threefold-higher loss rate of the AOA relative to NOB in the dark ocean allow for approximately equally low ammonia and nitrite concentrations at depth amid homeostasis of the two-step nitrification process. Moreover, the matched high affinity of AOA and NOB may allow the system to be maintained closer to homeostasis more often, given time-varying rates of surface primary production and subsequent export of reduced N to depth.

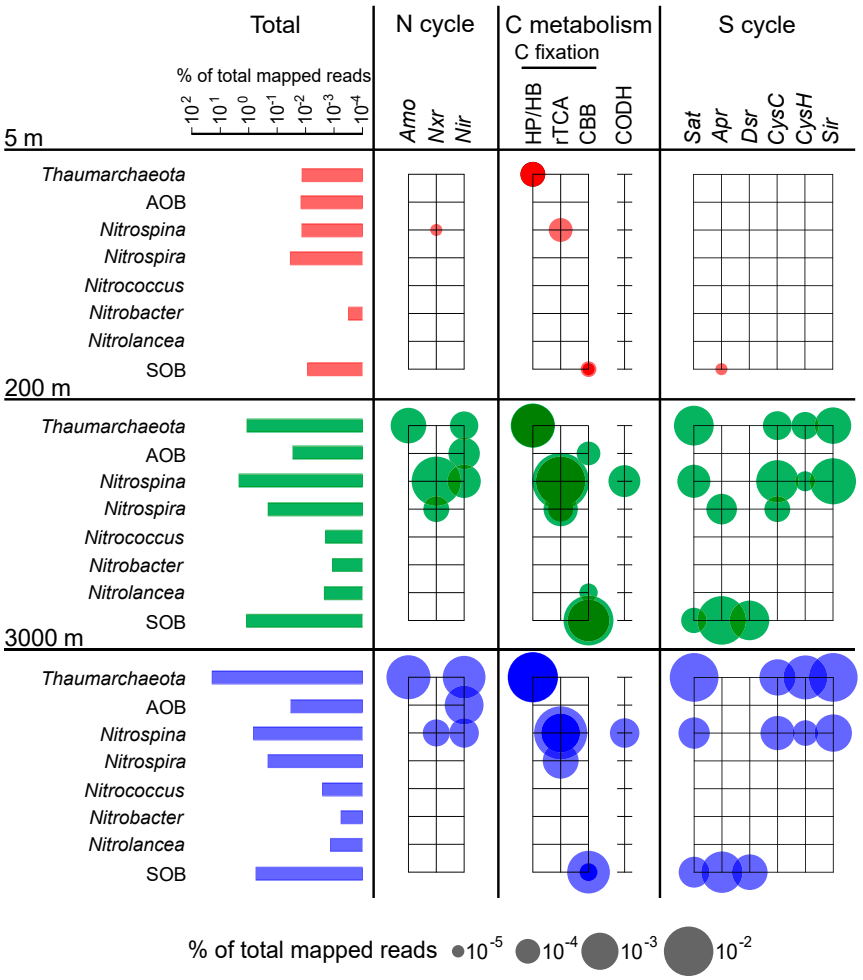

Fig. 4. Gene transcription in AOA and NOB. Relative transcript abundances of phylogenetic taxa and of genes encoding enzymes involved in the N cycle, C metabolism, and sulfur cycle in metatranscriptomes are shown. For the C-fixation pathway, dark circles indicate relative transcript abundances of genes encoding essential/key enzymes (*SI Appendix*, Table S2); light circles indicate relative transcript abundances of all genes encoding enzymes involved in each pathway. *Amo*, ammonia monooxygenase; *Apr*, adenylylsulfate reductase; CBB, Calvin Benson Basham cycle; *CysC*, adenylyl-sulfate kinase; *CysH*, phosphoadenosine phosphosulfate reductase; *Dsr*, dissimilatory sulfite reductase; *Nir*, nitrite reductase; *Nxr*, nitrite oxidoreductase; *Sat*, sulfate adenylyltransferase; *Sir*, sulfite reductase; SOB, sulfur-oxidizing bacteria.

Collectively, homeostasis in the lower epipelagic and mesopelagic N cycle is characterized by an interplay of contrasting life strategies of ammonia- and nitrite-oxidizing microbial assemblages with similar affinities maintaining nearly equal oxidation rates of their respective N substrates in the energy-poor environment of the dark ocean. Our analysis suggests that chemoautotrophic nitrification is associated with a global C-fixation rate of $\sim 1 \times 10^{13}$ to $\sim 2 \times 10^{13}$ mol of C per year in the dark ocean.

Materials and Methods

Oceanographic Observations. Seawater samples were collected from the SCS during research cruises in September 2014, May 2016, and June 2017, as well as from the WP during research cruises in April and August 2015 (*SI Appendix*, Fig. S1). Nutrient concentrations below the nitracline were measured by using a four-channel continuous-flow Technicon AA3 Auto-Analyzer. The detection limits for NO_3^- and NO_2^- were 0.1 and 0.04 μmol·L^{-1}, respectively, with a precision better than 1% and 3%. For samples collected above the nitracline, NO_3^- and NO_2^- concentrations were determined by the standard colorimetric method coupled with a flow-injection analysis–liquid waveguide capillary cell system (World Precision Instruments) (44); the detection limit was 5 nmol·L^{-1}, and precision was better than 3.1%. NH_4^+ concentrations were measured on board by using a modified fluorometric method with a detection limit of 1.2 nmol·L^{-1} and a precision of ±3.5% (45).

Abundances of the archaeal and β-proteobacterial *amoA* genes, thaumarchaeal (MGI) 16S rRNA genes, *Nitrospira* and *Nitrospina* 16S rRNA genes, and archaeal *accA* genes were quantified by using qPCR. For each sample, about 100 L of seawater was collected for metatranscriptomics analysis. De novo assembly of the quality-filtered reads was performed by using Trinity with default settings (46). The unigenes were blasted against public databases, including National Center for Biotechnology Information (NCBI) nonredundant protein, Swiss-Prot, Kyoto Encyclopedia of Genes and Genomes, Clusters of Orthologous Groups, and Gene Ontology (BLASTX; E value < 10^{-5}). To assess the quality of assembly, reads of each sample were mapped back to the merged unigenes by using Bowtie2 (Version 2.2.5) with the setting of one mismatch in the seed alignment (47). Detailed information on the experimental procedures and functional assignments can be found in *SI Appendix*, *Materials and Methods*.

Incubations to determine ammonia- and nitrite-oxidation rates were conducted on deck by using the ^{15}N-labeling technique. All incubations were carried out in the dark at in situ (±1 °C) temperature for 12 h. Each incubation was performed in triplicate. $\delta^{15}N$ of NO_2^- was determined by using the azide-reduction method (48). $\delta^{15}N$ of NO_3^- was determined by using the bacterial method (49). The N_2O converted from NO_2^- or NO_3^- was introduced to a gas-chromatography isotope ratio mass spectrometry (IRMS; Thermo Delta V Advantage) coupled with an online N_2O cryogenic extraction and purification system. Accuracy (pooled SD) was better than ±0.2‰ for the bacterial method and ±0.4‰ for the azide-reduction method. Ammonia- and nitrite-oxidation rates were primarily determined by the accumulation of ^{15}N in the product pool relative to the initial. For

ammonia- and nitrite-oxidation kinetics, the dependence of NH_4^+ or NO_2^- oxidation rates on substrate concentration was investigated by using five different concentrations of ^{15}N–NH_4^+ (0.03, 0.048, 0.096, 0.4, and 2 μM; 98% of ^{15}N atom; Sigma-Aldrich) or ^{15}N–NO_2^- (0.03, 0.1, 0.2, 0.5, and 2 μM; 98% of ^{15}N atom; Sigma-Aldrich). Time-series incubations were carried out in a thermostat incubator at in situ (±1 °C) temperature in the dark. Incubations were performed in duplicate. $\delta^{15}N$ of NO_2^- and NO_3^- was measured as described above. Detailed information on the experimental procedures and the equations to quantify the transformation rate of bulk substrate and estimate the kinetics constants (V_{max} and K_s) can be found in *SI Appendix, Materials and Methods*.

Laboratory Experiments. Incubation experiments with the strains *N. maritimus* SCM1, *N. moscoviensis* NSP M-1, and *N. gracilis* 3/211 (*SI Appendix, Materials and Methods*) were set up in a total of 155 polycarbonate bottles (500 mL volume) or Erlenmeyer flasks (300 mL volume), with initial cell abundances of ~6×10^5, ~1×10^6, and 6×10^5 to 7×10^5 cells per mL. Samples were generally collected in the exponential and stationary phase at 1- to 2-d intervals. Cell abundances were determined by using an Accuri C6 flow cytometer (BD Biosciences). DNA and RNA were extracted by using an All Prep DNA and RNA extraction kit (Qiagen). The concentration of inorganic N species was determined as described above. Ammonia- and nitrite-oxidation rates were measured by using ^{15}N–NH_4^+ and ^{15}N–NO_2^-, respectively. The tracer concentrations were about 10% of substrate concentration. DIC-fixation rates were quantified by using ^{13}C–HCO_3^- as tracer with a concentration of around 100 μmol·L^{-1}. The concentrations and $\delta^{15}N$ of nitrite and nitrate were measured as described above, and $\delta^{13}C$ of particulate organic C was measured by using an elemental-analyzer IRMS (Thermo Finnigan Flash EA 2000 interfaced to an Delta V^{PLUS} isotopic ratio mass spectrometer) system with a precision < ±0.4‰.

Steady-State Nitrification Balances in the Dark Ocean. We examined the steady-state balances from the microbial ecosystem model of Zakem et al. (25) with explicit nitrifying populations. We included only the terms applicable to the aphotic zone (i.e., no phytoplankton), and we assumed no transport. With these simplifications, relevant equations for the nitrification system in the dark ocean are:

$$\frac{dNH_4^+}{dt} = \left(\frac{1}{y_D} - 1\right)\mu_{het}B_{het} - \frac{1}{y_{NH_4}}\mu_{AOA}B_{AOA}, \quad [1]$$

$$\frac{dNO_2^-}{dt} = \left(\frac{1}{y_{NH_4}} - 1\right)\mu_{AOA}B_{AOA} - \frac{1}{y_{NO_2}}\mu_{NOB}B_{NOB}, \quad [2]$$

$$\frac{dB_{AOA}}{dt} = B_{AOA}(\mu_{AOA} - L_{AOA}), \quad [3]$$

$$\frac{dB_{NOB}}{dt} = B_{NOB}(\mu_{NOB} - L_{NOB}), \quad [4]$$

where B_{het}, B_{AOA}, and B_{NOB} (mol of N per liter) are the biomasses of heterotrophic bacteria, ammonia-oxidizing organisms, and nitrite-oxidizing organisms, respectively. Growth rate μ_i (d^{-1}) and loss rate L_i are specific for each population i. Here, we neglect explicit representation of zooplankton, though for our purposes, B_{het} may represent the total heterotrophic population, both zooplankton and microbial. Yield y_i (mol of biomass N per mol of DIN or organic detritus utilized) is the yield with respect to biomass for each population. D represents organic detritus.

Nitrifier growth rates. As in Zakem et al. (25), growth rate μ (d^{-1}) for each microbial population is expressed as a function of the yield y (mol of biomass N per mol of utilized N), the maximum specific resource uptake rate V_{max} (mol of N per mol of biomass N per d), and a half-saturation concentration K (mol of N per liter). For the two nitrifying populations, the modeled growth rates are:

$$\mu_{AOA} = \mu_{AOA}^{max}\frac{[NH_4^+]}{K_{NH_4} + [NH_4^+]} = y_{NH_4}V_{max}\frac{[NH_4^+]}{K_{NH_4} + [NH_4^+]}, \quad [5]$$

$$\mu_{NOB} = \mu_{NOB}^{max}\frac{[NO_2^-]}{K_{NO_2} + [NO_2^-]} = y_{NO_2}V_{max}\frac{[NO_2^-]}{K_{NO_2} + [NO_2^-]}, \quad [6]$$

where μ_{AOA}^{max} and μ_{NOB}^{max} are the maximum growth rates (yV_{max}). At steady state, the growth rate equals the loss rate ($\mu_i = L_i$) when the population is sustainable in the environment.

Ammonia and nitrite concentrations. Using the resource ratio framework (50, 51), the ambient concentrations of ammonia and nitrite can be related to the nitrifier yields, loss rates, and uptake kinetic parameters. As outlined in Zakem et al. (25), the subsistence concentration (R^*) that limits the growth of each nitrifying population is:

$$R^* = \frac{KL}{yV_{max} - L}. \quad [7]$$

For simplification, we can assume that the maximum growth rate is substantially higher than the loss rate, and so neglect L in the denominator, and we can refer to substrate affinity $V_{max}K^{-1}$ as affinity α. This gives the ratio of ammonia to nitrite at steady state as:

$$[NH_4^+]^* : [NO_2^-]^* = \frac{y_{NO_2}}{y_{NH_4}}\frac{L_{AOA}}{L_{NOB}}\frac{\alpha_{NOB}}{\alpha_{AOA}}. \quad [8]$$

The published model solutions (25) predicted that nitrite concentrations should be higher than ammonia concentrations at depth due to a threefold difference in efficiency if uptake kinetics and affinities (V_{max} and K) are equal. This reflected a parameterization of loss rates that resulted in equal specific loss rates (balanced by the in situ growth rates) for the two populations. According to Eq. **8**, if the yield is threefold higher for ammonia-oxidizers, and all else is equal, $[NH_4^+]^*$:$[NO_2^-]^*$ is ~1:3. If the loss rate is also threefold higher, then $[NH_4^+]^*$:$[NO_2^-]^*$ is ~1:1, matching our observations. Thus, we use a combination of theory and observations to provide a constraint on the loss rates of the nitrifying populations in the deep ocean.

Bulk nitrification rates. Assuming $(1 - y_D) \approx (1 - y_{NH4}) \approx 1$, Eqs. **1** and **2** can be approximated as:

$$\frac{dNH_4^+}{dt} \approx \frac{1}{y_D}\mu_{het}B_{het} - \frac{1}{y_{NH_4}}\mu_{AOA}B_{AOA}, \quad [9]$$

$$\frac{dNO_2^-}{dt} \approx \frac{1}{y_{NH_4}}\mu_{AOA}B_{AOA} - \frac{1}{y_{NO_2}}\mu_{NOB}B_{NOB}. \quad [10]$$

At steady state ($dNH_4^+/dt = dNO_2^-/dt = 0$), Eqs. **9** and **10** can be combined as:

$$\frac{1}{y_D}\mu_{het}B_{het} = \frac{1}{y_{NH_4}}\mu_{AOA}B_{AOA} = \frac{1}{y_{NO_2}}\mu_{NOB}B_{NOB}, \quad [11]$$

where the left term is the excretion rate of ammonia by heterotrophs, the center term is the ammonia-oxidation rate, and the right term is the nitrite-oxidation rate. This indicates that the ammonia- and nitrite-oxidation rates must be equal when the steady-state approximation is valid, pending no other sinks of ammonia or sources or sinks of nitrite, and, furthermore, that these nitrification rates must equal the rate of ammonia excretion from associated heterotrophic consumption of organic matter.

Nitrifier biomass and abundances. From Eq. **11**, and assuming steady-state growth for the microbial populations ($\mu_i = L_i$), we can derive an expression for the relative biomass concentrations of the two nitrifying populations as:

$$\frac{B_{AOA}}{B_{NOB}} = \frac{y_{NH_4}}{y_{NO_2}}\frac{L_{NOB}}{L_{AOA}}. \quad [12]$$

Our observations match the redox-based estimate that y_{NH4} for AOA is about threefold higher than y_{NO2} for NOB. Above, we also speculated that the loss rate L_{AOA} may be threefold higher than L_{NOB} at depth. Inserting these equivalencies into Eq. **12** suggests that the biomasses of the two populations may be approximately equal $\left(\frac{B_{AOA}}{B_{NOB}} \approx 1\right)$.

Cell abundances X (cells per liter) can be calculated from biomass concentration B (mol of biomass N per liter) with an estimate of cell quota Q (mol of N per cell) as $X = BQ^{-1}$. Thus, the relative cellular abundances of the two nitrifying populations can be estimated as:

$$\frac{X_{AOA}}{X_{NOB}} = \frac{B_{AOA}}{B_{NOB}}\frac{Q_{NOB}}{Q_{AOA}}. \quad [13]$$

If NOB is much larger (i.e., has a larger quota) than AOA, then cellular abundances of AOA will be much higher, even if biomasses are equal. An estimated a 10-fold higher N cell quota for NOB than AOA (25) predicts that AOA should have a 10-fold higher cell abundance than NOB, which is consistent with our observations.

Data Availability. Data supporting the findings of this study are available in this article and *SI Appendix*. The metatranscriptomics data sets were deposited in the Short Reads Archive (NCBI) under accession nos. SRR5518753, SRR5515070, and SRR5518752. The transcriptome shotgun assembly project was deposited at DNA Data Bank of Japan/European Molecular Biology

ECOLOGY

Laboratory/GenBank under the accession no. GGEF00000000. The version described in this paper is the first version, GGEF00000000. The Fortran code for the MATLAB code for the thermodynamic analyses are available at https://github.com/emilyzakem/ZhangLabXMU.

ACKNOWLEDGMENTS. We thank E. Spieck (University of Hamburg) for providing the 3/211, Nb-231, and NSP M-1 strains; and C. L. Zhang for providing the SCM1 strain. We also thank Y. Zhang for assistance in sampling; Z. Chen, Z. Zuo, and D. Zhao for assistance in DNA/RNA extraction and qPCR measurements; and T. Huang for assistance in ammonia-concentration measurements on board. The two anonymous referees and the handling editor are thanked for their critical and constructive reviews. We especially sincerely thank one of the reviewers for the constructive analysis of this paper that helped the biogeochemical model. This work was supported by National Key Research and Development Program Grant 2016YFA0601400; National Natural Science Foundation of China (NSFC) Major Program 91751207; National Key Scientific Research Project 2015CB954000; and NSFC Projects 41721005, 91428308, and 41676125. W.Q. was supported by Simons Postdoctoral Fellowship in Marine Microbial Ecology 548565. E.J.Z. was supported by the Simons Postdoctoral Fellowship in Marine Microbial Ecology. D.A.S. was supported by NSF Dimensions of Biodiversity Program Grant OCE-1046017. G.J.H. was supported by Austrian Science Fund (FWF) Projects ARTEMIS (P 28781-B21) and "Microbial Nitrogen Cycling: From Single Cells to Ecosystems" (W1257-B20). A.E.I. was supported by grants from the Simons Foundation (SCOPE Award ID 329108). This study is a contribution to the international Integrated Marine Biosphere Research project.

1. N. Gruber, "The marine nitrogen cycle: Overview and challenges" in *Nitrogen in the Marine Environment*, D. G. Capone, D. A. Bronk, M. R. Mulholland, E. J. Carpenter, Eds. (Elsevier, Amsterdam, The Netherlands, ed. 2, 2008), pp. 1–50.
2. H. Daims *et al*., Complete nitrification by *Nitrospira* bacteria. *Nature* **528**, 504–509 (2015).
3. M. A. H. J. van Kessel *et al*., Complete nitrification by a single microorganism. *Nature* **528**, 555–559 (2015).
4. A. J. Pinto *et al*., Metagenomic evidence for the presence of comammox *Nitrospira*-like bacteria in a drinking water system. *MSphere* **1**, e00054-15 (2015).
5. E. Costa, J. Pérez, J.-U. Kreft, Why is metabolic labour divided in nitrification? *Trends Microbiol.* **14**, 213–219 (2006).
6. J. E. Dore, D. M. Karl, Nitrite distributions and dynamics at station ALOHA. *Deep Sea Res. Part II Top. Stud. Oceanogr.* **43**, 385–402 (1996).
7. B. B. Ward, D. G. Capone, J. P. Zehr, What's new in the nitrogen cycle? *Oceanography* **20**, 101–109 (2007).
8. A. E. Santoro *et al*., Measurements of nitrite production in and around the primary nitrite maximum in the central California Current. *Biogeosciences* **10**, 7395–7410 (2013).
9. P. Lam *et al*., Origin and fate of the secondary nitrite maximum in the Arabian Sea. *Biogeosciences* **8**, 1565–1577 (2011).
10. W. Martens-Habbena, P. M. Berube, H. Urakawa, J. R. de la Torre, D. A. Stahl, Ammonia oxidation kinetics determine niche separation of nitrifying Archaea and Bacteria. *Nature* **461**, 976–979 (2009).
11. M. G. Pachiadaki *et al*., Major role of nitrite-oxidizing bacteria in dark ocean carbon fixation. *Science* **358**, 1046–1051 (2017).
12. T. J. Mincer *et al*., Quantitative distribution of presumptive archaeal and bacterial nitrifiers in Monterey Bay and the North Pacific Subtropical Gyre. *Environ. Microbiol.* **9**, 1162–1175 (2007).
13. T. Nunoura *et al*., Hadal biosphere: Insight into the microbial ecosystem in the deepest ocean on Earth. *Proc. Natl. Acad. Sci. U.S.A.* **112**, E1230–E1236 (2015).
14. A. E. Santoro, K. L. Casciotti, C. A. Francis, Activity, abundance and diversity of nitrifying archaea and bacteria in the central California Current. *Environ. Microbiol.* **12**, 1989–2006 (2010).
15. X. Peng *et al*., Revisiting nitrification in the Eastern Tropical South Pacific: A focus on controls. *J. Geophys. Res. Oceans* **121**, 1667–1684 (2016).
16. R. E. Horak *et al*., Ammonia oxidation kinetics and temperature sensitivity of a natural marine community dominated by Archaea. *ISME J.* **7**, 2023–2033 (2013).
17. S. E. Newell, S. E. Fawcett, B. B. Ward, Depth distribution of ammonia oxidation rates and ammonia-oxidizer community composition in the Sargasso Sea. *Limnol. Oceanogr.* **58**, 1491–1500 (2013).
18. X. S. Wan *et al*., Ambient nitrate switches the ammonium consumption pathway in the euphotic ocean. *Nat. Commun.* **9**, 915 (2018).
19. K. D. Kits *et al*., Kinetic analysis of a complete nitrifier reveals an oligotrophic lifestyle. *Nature* **549**, 269–272 (2017).
20. J. Jacob *et al*., Oxidation kinetics and inverse isotope effect of marine nitrite-oxidizing isolates. *Aquat. Microb. Ecol.* **80**, 289–300 (2017).
21. B. Nowka, H. Daims, E. Spieck, Comparison of oxidation kinetics of nitrite-oxidizing bacteria: Nitrite availability as a key factor in niche differentiation. *Appl. Environ. Microbiol.* **81**, 745–753 (2015).
22. D. Y. Sorokin *et al*., Nitrification expanded: Discovery, physiology and genomics of a nitrite-oxidizing bacterium from the phylum *Chloroflexi*. *ISME J.* **6**, 2245–2256 (2012).
23. X. Sun, Q. Ji, A. Jayakumar, B. B. Ward, Dependence of nitrite oxidation on nitrite and oxygen in low-oxygen seawater. *Geophys. Res. Lett.* **44**, 7883–7891 (2017).
24. W. Qin *et al*., *Nitrosopumilus maritimus* gen. nov., sp. nov., *Nitrosopumilus cobalaminigenes* sp. nov., *Nitrosopumilus oxyclinae* sp. nov., and *Nitrosopumilus ureiphilus* sp. nov., four marine ammonia-oxidizing archaea of the phylum Thaumarchaeota. *Int. J. Syst. Evol. Microbiol.* **67**, 5067–5079 (2017).
25. E. J. Zakem *et al*., Ecological control of nitrite in the upper ocean. *Nat. Commun.* **9**, 1206–1218 (2018).
26. X. Peng *et al*., Nitrogen uptake and nitrification in the subarctic North Atlantic Ocean. *Limnol. Oceanogr.* **63**, 1462–1487 (2018).
27. D. R. Clark, A. P. Rees, I. Joint, Ammonium regeneration and nitrification rates in the oligotrophic Atlantic Ocean: Implications for new production estimates. *Limnol. Oceanogr.* **53**, 52–62 (2008).
28. B. B. Ward, Nitrogen transformations in the Southern California Bight. *Deep-Sea Res.* **34**, 785–805 (1987).
29. B. B. Ward, "Nitrification in marine systems" in *Nitrogen in the Marine Environment*, D. G. Capone, D. A. Bronk, M. R. Mulholland, E. J. Carpenter, Eds. (Elsevier, Amsterdam, The Netherlands, ed. 2, 2008), pp. 199–262.
30. M. H. Conte, N. Ralph, E. H. Ross, Seasonal and interannual variability in deep ocean particle fluxes at the Oceanic Flux Program (OFP)/Bermuda Atlantic Time Series (BATS) site in the western Sargasso Sea near Bermuda. *Deep Sea Res. Part II Top. Stud. Oceanogr.* **48**, 1471–1505 (2001).
31. S. Roux *et al*.; Tara Oceans Coordinators, Ecogenomics and potential biogeochemical impacts of globally abundant ocean viruses. *Nature* **537**, 689–693 (2016).
32. N. A. Ahlgren, C. A. Fuchsman, G. Rocap, J. A. Fuhrman, Discovery of several novel, widespread, and ecologically distinct marine *Thaumarchaeota* viruses that encode *amoC* nitrification genes. *ISME J.* **13**, 618–631 (2019).
33. R. Danovaro *et al*., Virus-mediated archaeal hecatomb in the deep seafloor. *Sci. Adv.* **2**, e1600492 (2016).
34. A. E. Santoro *et al*., Thaumarchaeal ecotype distributions across the equatorial Pacific Ocean and their potential roles in nitrification and sinking flux attenuation. *Limnol. Oceanogr.* **62**, 1984–2003 (2017).
35. J. M. Smith, J. Damashek, F. P. Chavez, C. A. Francis, Factors influencing nitrification rates and the abundance and transcriptional activity of ammonia oxidizing microorganisms in the dark northeast Pacific Ocean. *Limnol. Oceanogr.* **61**, 596–609 (2016).
36. B. B. Ward, O. C. Zafiriou, Nitrification and nitric oxide in the oxygen minimum of the eastern tropical North Pacific. *Deep Sea Res.* **35**, 1127–1142 (1988).
37. C. Wuchter *et al*., Archaeal nitrification in the ocean. *Proc. Natl. Acad. Sci. U.S.A.* **103**, 12317–12322 (2006).
38. P. A. del Giorgio, C. M. Duarte, Respiration in the open ocean. *Nature* **420**, 379–384 (2002).
39. F. J. Stewart, O. Ulloa, E. F. DeLong, Microbial metatranscriptomics in a permanent marine oxygen minimum zone. *Environ. Microbiol.* **14**, 23–40 (2012).
40. S. Ganesh *et al*., Size-fraction partitioning of community gene transcription and nitrogen metabolism in a marine oxygen minimum zone. *ISME J.* **9**, 2682–2696 (2015).
41. G. M. King, C. F. Weber, Distribution, diversity and ecology of aerobic CO-oxidizing bacteria. *Nat. Rev. Microbiol.* **5**, 107–118 (2007).
42. J. C. Xavier, M. Preiner, W. F. Martin, Something special about CO-dependent CO_2 fixation. *FEBS J.* **285**, 4181–4195 (2018).
43. J. A. Raven, Contributions of anoxygenic and oxygenic phototrophy and chemolithotrophy to carbon and oxygen fluxes in aquatic environments. *Aquat. Microb. Ecol.* **56**, 177–192 (2009).
44. J. Zhang, Shipboard automated determination of trace concentrations of nitrite and nitrate in oligotrophic water by gas-segmented continuous flow analysis with a liquid waveguide capillary flow cell. *Deep Sea Res. Part I Oceanogr. Res. Pap.* **47**, 1157–1171 (2000).
45. Y. Zhu, D. Yuan, Y. Huang, J. Ma, S. Feng, A sensitive flow-batch system for on board determination of ultra-trace ammonium in seawater: Method development and shipboard application. *Anal. Chim. Acta* **794**, 47–54 (2013).
46. M. G. Grabherr *et al*., Full-length transcriptome assembly from RNA-seq data without a reference genome *Nat. Biotechnol.* **29**, 644–652 (2011).
47. B. Langmead, C. Trapnell, M. Pop, S. L. Salzberg, Ultrafast and memory-efficient alignment of short DNA sequences to the human genome. *Genome Boil.* **10**, R25 (2009).
48. M. R. McIlvin, M. A. Altabet, Chemical conversion of nitrate and nitrite to nitrous oxide for nitrogen and oxygen isotopic analysis in freshwater and seawater. *Anal. Chem.* **77**, 5589–5595 (2005).
49. D. M. Sigman *et al*., A bacterial method for the nitrogen isotopic analysis of nitrate in seawater and freshwater. *Anal. Chem.* **73**, 4145–4153 (2001).
50. F. M. Stewart, B. R. Levin, Partitioning of resources and the outcome of interspecific competition: A model and some general considerations. *Am. Nat.* **107**, 171–196 (1973).
51. D. Tilman, *Resource Competition and Community Structure* (Princeton University Press, Princeton, NJ, 1982).
52. Y. Suwa, Y. Imamura, T. Suzuki, T. Tashiro, Y. Urushigawa, Ammonia-oxidizing bacteria with different sensitivities to $(NH_4)_2SO_4$ in activated sludges. *Water Res.* **28**, 1523–1532 (1994).
53. J. Groeneweg, B. Sellner, W. Tappe, Ammonia oxidation in *Nitrosomonas* at NH_3 concentrations near K_m: Effects of pH and temperature. *Water Res.* **28**, 2561–2566 (1994).
54. A. Bollmann, M. J. Bär-Gilissen, H. J. Laanbroek, Growth at low ammonium concentrations and starvation response as potential factors involved in niche differentiation among ammonia-oxidizing bacteria. *Appl. Environ. Microbiol.* **68**, 4751–4757 (2002).
55. T. E. Koper, J. M. Stark, M. Y. Habteselassie, J. M. Norton, Nitrification exhibits Haldane kinetics in an agricultural soil treated with ammonium sulfate or dairy-waste compost. *FEMS Microbiol. Ecol.* **74**, 316–322 (2010).
56. Q. Q. Jiang, L. R. Bakken, Comparison of *Nitrosospira* strains isolated from terrestrial environments. *FEMS Microbiol. Ecol.* **30**, 171–186 (1999).